

**Observation of optical Smith-Purcell radiation at an electron beam energy of 855 MeV**

G. Kube,\* H. Backe, H. Euteneuer, A. Grendel, F. Hagenbuck, H. Hartmann, K. H. Kaiser, W. Lauth,  
H. Schöpe, G. Wagner, and Th. Walcher  
*Institut für Kernphysik, Universität Mainz, D-55099 Mainz, Germany*

M. Kretzschmar  
*Institut für Physik, Universität Mainz, D-55099 Mainz, Germany*  
(Received 18 December 2001; published 8 May 2002)

Smith-Purcell radiation, generated when a beam of charged particles passes close to the surface of a diffraction grating, has been studied in the visible spectral range at wavelengths of 360 and 546 nm with the low emittance 855 MeV electron beam of the Mainz Microtron MAMI. The beam focused to a spot size of 4  $\mu\text{m}$  (full width at half maximum) passed over optical diffraction gratings of echelle profiles with blaze angles of  $0.8^\circ$ ,  $17.27^\circ$ , and  $41.12^\circ$  and grating periods of 0.833 and 9.09  $\mu\text{m}$ . Taking advantage of the specific emission characteristics of Smith-Purcell radiation a clear separation from background components, such as diffracted synchrotron radiation from upstream beam optical elements and transition radiation, was possible. The intensity scales with a modified Bessel function of the first kind as a function of the distance between electron beam and grating surface. Experimental radiation factors have been determined and compared with calculations on the basis of Van den Berg's theory [P.M. Van den Berg, *J. Opt. Soc. Am.* **63**, 689 (1973)]. Fair agreement has been found for gratings with large blaze angles while the measurement with the shallow grating (blaze angle  $0.8^\circ$ ) is at variance with this theory. Finally, the optimal operational parameters of a Smith-Purcell radiation source in view of already existing powerful undulator sources are discussed.

DOI: 10.1103/PhysRevE.65.056501

PACS number(s): 41.60.-m, 42.25.Fx, 42.79.Dj

**I. INTRODUCTION**

Smith-Purcell (SP) radiation is generated when a beam of charged particles passes close to the surface of a periodic structure, i.e., a diffraction grating. The radiation mechanism was predicted by Frank in 1942 [1] and observed in the visible spectral range for the first time by Smith and Purcell [2]. They used a 250–300 keV electron beam with a typical current of several microampere. In a number of subsequent experiments the results were confirmed mainly in the visible spectral range [3–9]. Soon after the discovery, potential applications of the SP effect also became the topic of interest. In a number of theoretical and experimental studies the SP effect has been discussed as a basis for free-electron lasers (e.g., [10–17]), for particle acceleration [18], or for particle beam diagnostics [19,20].

For low-electron energies and small wavelengths the coupling of the electron beam to the grating surface rapidly weakens if the distance between the electron beam and the grating increases. To achieve a sufficient radiation output in most of the experiments the electron beam scratched the grating surface making it impossible to distinguish between SP radiation and competitive mechanisms as, for example, transition radiation production at the grating structures. This fact was probably one of the reasons why the intensity of SP radiation was controversially discussed in a number of papers (see, e.g., [3,21–24]). Later on, experiments with larger electron energies and longer wavelengths

were reported [25–29]. At energies in the mega-electron-volt range or even more the distance between electron beam and grating surface can be increased and, therefore, competing production mechanisms arising from the interaction of the electrons with the grating can widely be avoided. Fair agreement was reported between the measured intensity in the far-infrared and millimeter spectral region and theoretical predictions [26,28–31].

The purpose of the experiments presented in this paper was to investigate the coupling of the virtual photon field of the electron to the grating at the ultrarelativistic energy of 855 MeV [32]. Radiation was generated with the low-emittance electron beam of the Mainz Microtron MAMI [33]. SP radiation in the visible spectral range was separated from background components such as diffracted synchrotron radiation from upstream beam optical elements and transition radiation. The latter is emitted when electrons traverse the grating grooves. The intensity of SP radiation is compared with theoretical calculations based on the theory of Van den Berg [34] and a scalar model developed in the course of this paper. The latter is described in the Appendix of this paper.

The paper is organized as follows. In Sec. II, the basic radiation characteristics of SP radiation with regard to ultrarelativistic electron energies are described. The experiments and the procedure to separate SP radiation from background components are described in Sec. III. In Sec. IV, the experimental radiation factors are compared with theoretical predictions. Section V is dedicated to the discussion about the operational parameters of a possible future SP radiation source in view of already existing powerful undulator radiation sources. A concluding section summarizes the paper.

---

\*Corresponding author. Fax: +49 6131 3922964; email address: Kube@kph.uni-mainz.de

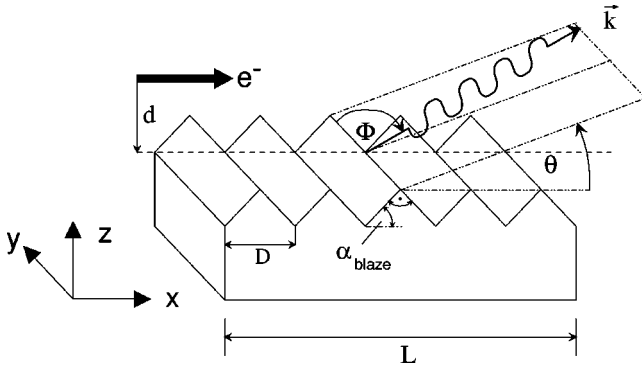


FIG. 1. Definition of the geometry. The electron moves with constant reduced velocity  $\beta=v/c$  at a distance  $d$  parallel to the grating surface in  $x$  direction. The grooves, oriented in the  $y$  direction, repeat periodically with the grating period  $D$ . The blaze angle  $\alpha_{blaze}$  characterizes the *échelette* gratings which we used in this paper. The direction of the photon wave-vector  $\vec{k}$  is described in the emission plane resulting from the  $z=0$  plane by a rotation about the  $y$  axis by the angle  $\theta$ . In the emission plane the  $\vec{k}$  vector makes an angle  $\Phi$  with the  $y$  axis. The length of the grating is denoted by  $L$ .

## II. DEFINITION AND CHARACTERISTICS OF SMITH-PURCELL RADIATION COMPONENT

In this paper, we designate as SP radiation only that radiation component which is emitted under the restriction that no electrons enter the grating surface. One characteristic signature of SP radiation in this sense is that it must fulfill the dispersion relation

$$\lambda = \frac{D}{|n|} (1/\beta - \cos \theta \sin \Phi). \quad (1)$$

In this equation,  $\lambda$  is the wavelength of the emitted radiation,  $D$  the grating period,  $n$  the diffraction order,  $\beta=v/c$  the reduced electron velocity, and  $\theta$ ,  $\Phi$  are the emission angles as introduced in Fig. 1. This relation was already deduced by Smith and Purcell [2] from a simple construction of Huygens elementary waves. In nearly all publications which appeared up to now it was argued that the experimental verification of Eq. (1) proves already the observation of SP radiation. However, the dispersion relation Eq. (1) is not at all a sufficient condition for SP radiation emission in the sense defined above. For example, the dispersion relation is also fulfilled for transition radiation emitted if an electron traverses the grooves of the grating. Therefore, an additional criterion must be found by which SP radiation can be identified unambiguously. This criterion will be formulated in the following.

According to the approach of di Francia [21] the radiation mechanism can be understood as the diffraction of the field of the electron by the grating. Above the grating surface this field is expanded in a set of evanescent plane waves which are scattered by the grating. Some of the scattered waves become propagating ones and can be observed as SP radiation. The angular distribution of the number of photons per electron radiated into the  $n$ th order is

$$\frac{dN}{d\Omega} = \alpha |n| N_w \frac{\sin^2 \theta \sin^2 \Phi}{(1/\beta - \cos \theta \sin \Phi)^2} |R_n|^2 \times \exp\left(-\frac{d}{h_{int}} \sqrt{1 + (\beta \gamma \cos \Phi)^2}\right), \quad (2)$$

where  $\alpha$  is the fine-structure constant,  $N_w$  the number of grating periods, and  $d$  the distance of the beam above the grating. The radiation factors  $|R_n|^2$  which are analogous to the reflection coefficients of optical gratings are a measure for the grating efficiency. They can be calculated by the theory of Van den Berg [34–39] which takes into account the shape of the groove profile. According to Eq. (2), the intensity decreases exponentially with increasing distance  $d$  between electron and grating surface. The interaction length

$$h_{int} = \frac{\lambda \beta \gamma}{4\pi}, \quad (3)$$

where  $\gamma=(1-\beta^2)^{-1/2}$  is the Lorentz factor, describes the characteristic finite range of the virtual photons emitted and reabsorbed by the electrons. Since the exponential in Eq. (2) is of fundamental origin this functional dependence on the distance can be chosen as a sufficient condition for the identification of SP radiation.

To achieve a good coupling between the electrons and the radiation field via the grating the mean spot size of the electron beam and its distance to the grating should be in the order of the interaction length  $h_{int}$ . However, in the experiment of Smith and Purcell [2] the beam spot size of 0.15 mm was much larger than the interaction length which was of order of  $h_{int} \approx 10^{-8}$  m. Such experimental conditions render an investigation of the radiation as a function of the distance impossible. At higher-beam energies, for instance, 855 MeV which is the current maximum energy of the Mainz Microtron MAMI, the interaction length in the optical spectral region amounts to  $h_{int} \approx 70$   $\mu\text{m}$ . Taking, in addition, advantage of the low-vertical emittance  $\varepsilon_z = 1$   $\pi$  nm rad of the MAMI electron beam, a beam spot size as small as a few micrometers can be achieved. With such parameters the investigation of SP radiation in the optical spectral region as a function of the distance seems to be promising.

Furthermore, at ultrarelativistic electron energies, the radiation is emitted according to Eq. (2) in a very narrow angular region around  $\Phi = 90^\circ$ , i.e., in the plane containing the grating normal and the electron beam. For typical parameters of our experiment,  $\lambda = 360$  nm and  $d = 100$   $\mu\text{m}$ , an angular width of  $\Delta\Phi = 1.0$  mrad [full width at half maximum (FWHM)] results. This feature can be used to discriminate SP radiation against background components as demonstrated later.

After this discussion of the main characteristics of SP radiation at ultrarelativistic electron energies we turn to the description of the experiment.

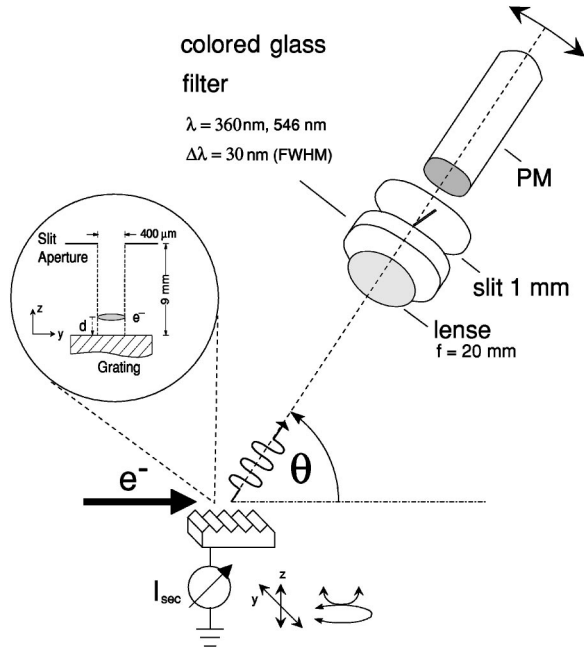


FIG. 2. Schematic picture of the experimental setup. The various degrees of freedom for the adjustment of the grating relative to the beam axis are indicated by the arrows. These are translational motions in  $y$ ,  $z$  direction and rotational motions around the  $y$ ,  $z$  axis. The distance between lens and grating is 195 mm. The insert depicts the slit aperture system in a cut perpendicular to the electron-beam direction.

### III. EXPERIMENT

#### A. Experimental setup and data taking

The setup of our experiment is shown in Fig. 2. The grating was mounted together with a beam diagnostic system, consisting of a wire scanner and a ZnS screen, on a four-axis goniometer which allowed the positioning of the grating with a translational and angular accuracy of  $1 \mu\text{m}$  and  $0.01^\circ$ , respectively, with respect to the electron beam. The aluminumized surface of the grating was electrically connected to a charge-sensitive preamplifier which measured the secondary electron signal  $I_{sec}$  released by beam electrons hitting the grating. In our experiments we investigated radiation emission from three gratings, designated as A, B, and C, whose parameters are listed in Table I.

At the position of the grating the 855 MeV electron beam was focused to a vertical spot size of  $\Delta z = 2 \mu\text{m}$  ( $1\sigma$ ). The

TABLE I. Parameters of the échelette-type replica gratings used in the experiments. The grating substrates consist of glass (BK7) covered with an aluminum coating of about  $(700 \pm 50)$  nm thickness. Manufacturer of grating A is Edmunds Scientific, Barrington, New York, of grating B and C, Milton Roy, Rochester, New York.

Grating	$\alpha_{blaze} [^\circ]$	D [ $\mu\text{m}$ ]	size [mm]
			L×W×H
A	17.27	0.833	25×25×10
B	41.12	0.833	20×20×10
C	0.8	9.09	30×30×10

divergence of the electron beam with an absolute vertical emittance of  $\varepsilon_z = 1 \pi \text{ nm rad}$  ( $1\sigma$ ) resulted in a larger effective spot size which was estimated from the envelope equation (see, e.g., [40]) to be  $3.4 \mu\text{m}$ . However, even this spot size is well below the interaction length  $h_{int} \approx 70 \mu\text{m}$ . In order to suppress detection of background signals in the photomultiplier tube the electron beam was pulsed with a repetition rate between 1 and 9 kHz and a pulse duration of 10 ns. The pulse current amounted typically to  $(58 \pm 2) \mu\text{A}$  and was measured via the calibrated induction voltage signal in a ferrite ring.

The detection system consisted of a photomultiplier tube (PM, Hamamatsu R647-P), a lens together with a slit which defined the accepted solid angle of the system, and a wavelength selecting color glass filter of bandwidth  $\Delta\lambda = 30 \text{ nm}$  (FWHM) in front of the multiplier. Two detection systems were mounted on a revolving spectrometer arm at the angle  $\Phi = 90^\circ$  permitting simultaneous measurements at the wavelengths  $\lambda = 360$  and  $\lambda = 546 \text{ nm}$ .

For the investigation of the dispersion relation Eq. (1) the gratings were positioned at a fixed distance  $d$  with respect to the beam and the angle  $\theta$  of the spectrometer arm was varied. For the investigation of the distance dependence the grating was moved step by step with the goniometric stage towards the electron beam with the detection system positioned at a fixed angle  $\theta_n$  as calculated by Eq. (1) and experimentally verified as the maximum before the measurements by a  $\theta$  scan.

#### B. Data analysis and extraction of SP radiation component

In Fig. 3, spectra are depicted which were taken as a function of the observation angle  $\theta$  at various grating positions  $d$ . The spectra show pronounced maxima at the positions which agree well with predictions of Eq. (1), i.e., the observed radiation satisfies the dispersion relation as a necessary condition. In the next step, it must be shown that the intensity as a function of the distance  $d$  obeys the exponential dependence of Eq. (2) which is the sufficient condition for the identification of SP radiation.

The intensity of the maxima as a function of the distance  $d$  is plotted in Fig. 4(a). For distances  $d \geq 25 \mu\text{m}$  the intensity for both wavelengths decreases exponentially alike to  $P_n = A \exp(-d/\Lambda)$  with a decay constant  $\Lambda \approx h_{int}$  as expected for SP radiation from Eq. (3). Notice that the slope is different for the two wavelengths which is also expected from Eq. (3). For distances  $d \leq 25 \mu\text{m}$  the same exponential dependence holds, however, with a very small  $\Lambda = 2.2 \mu\text{m}$  which is comparable with the vertical beam spot size. In Fig. 4(b) the secondary electron signal from the grating surface is plotted. The fact that the radiation component for  $0 < d < 25 \mu\text{m}$  correlates with both, the secondary electron signal and the vertical beam spot size, strongly suggests that this radiation component is optical transition radiation (OTR) produced by electrons of the beam halo traversing the grating grooves. The experimental proof of this conjecture is given in Ref. [41], further experiments and theoretical studies are described elsewhere [42,43]. As already mentioned the same dispersion relation Eq. (1) as for SP radiation holds also for

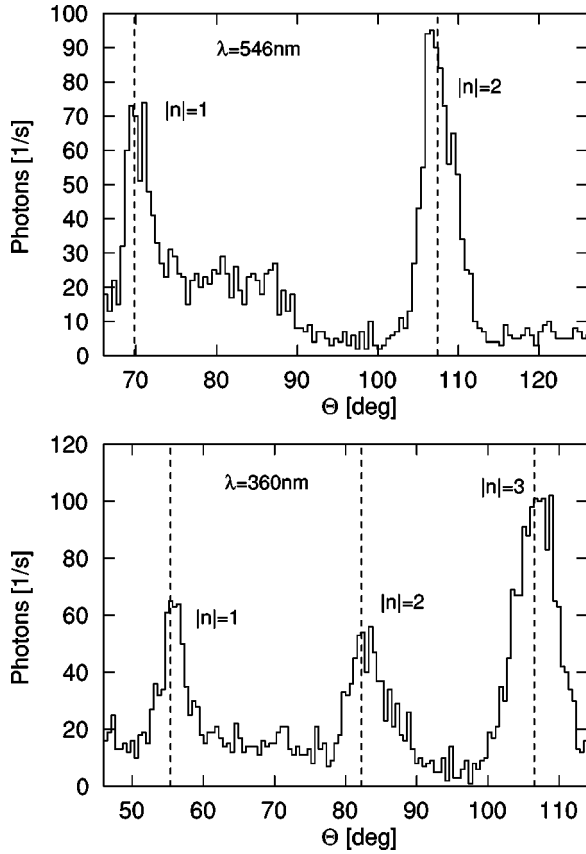


FIG. 3. Experimental photon intensity as a function of the observation angle  $\theta$ . The measurements were performed with grating B at a distance  $d=127 \mu\text{m}$  between electron beam and grating surface. The dashed vertical lines denote the calculated positions of the diffraction orders  $|n|=1,2,3$  according to Eq. (1). Tilt angle of the grating  $\alpha=0^\circ$ .

OTR. Consequently, in the following discussion only the radiation component at  $d \geq 25 \mu\text{m}$  is considered to be a candidate for SP radiation.

It remains to be proven that the radiation observed for distances  $d \geq 25 \mu\text{m}$  does not originate from synchrotron radiation (SR), produced in upstream beam optical components and diffracted by the grating. A detailed analysis of the beam optics showed that the quadrupole doublet directly in front of the grating is the strongest source of SR. This doublet was used to focus the beam to the required small spot size. To suppress this radiation a slit aperture was installed 9 mm above the grating, see Fig. 2. The slit with a width of  $400 \mu\text{m}$  was oriented parallel to the beam direction. The corresponding angular width of the accepted radiation of  $\Delta\Phi=44 \text{ mrad}$  was large enough to accept the strongly directional emitted SP radiation. With this aperture, the SR background component was reduced but could not be completely suppressed.

The principle of the procedure to separate the remaining SR and SP radiation components will be explained by means of Fig. 5. If the grating is tilted by an angle  $\alpha$  with respect to the beam direction the intensity of SP radiation varies sym-

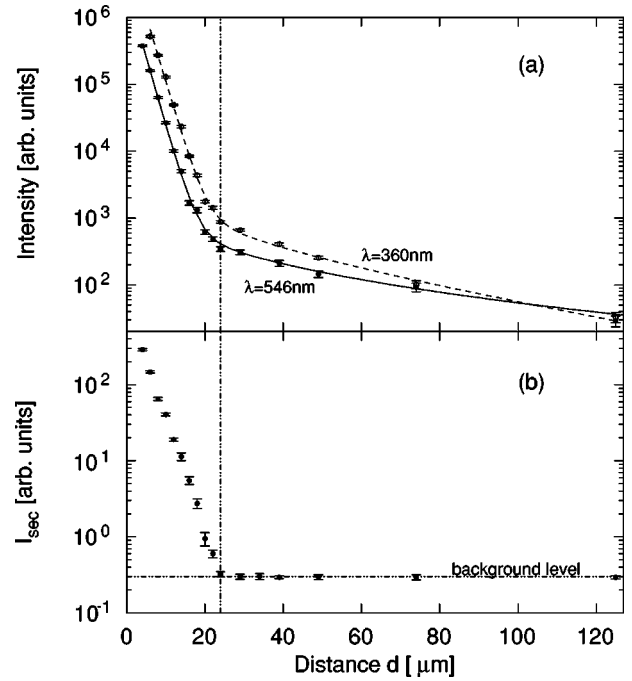


FIG. 4. (a) Observed radiation intensity for wavelengths  $\lambda = 360 \text{ nm}$  and  $546 \text{ nm}$  at first order and (b) secondary electron signal as a function of the distance between electron beam and grating. Measurements were performed with grating B at fixed observation angle  $\theta_1 = 55.4^\circ$  and  $\theta_1 = 69.8^\circ$  for the wavelengths  $360 \text{ nm}$  and  $546 \text{ nm}$ , respectively. The correlation of the intensity with the secondary electron signal for  $d \leq 25 \mu\text{m}$  indicates that this radiation component is optical transition radiation.

metrically with respect to  $\alpha=0^\circ$ , the angle at which the grating surface is aligned with respect to the beam direction. In contrast, the diffracted SR intensity is strongest if the grating is tilted towards the upstream direction and vanishes if tilted in the opposite direction.

The experimental observation is in accord with this expectation as demonstrated by Fig. 6. From this picture it is obvious that the SP radiation should be separable from the diffracted SR component. The procedure is based on the functional dependency of the intensity  $N(d, \alpha)$  on the beam distance  $d$  from the grating and on the tilt angle  $\alpha$ . A typical spectrum is shown in Fig. 7. Each of these spectra must be decomposed into the desired SP radiation component  $N_{SP}(d, \alpha)$ , a possible diffracted SR component  $N_{SR}(d, \alpha)$ , and a background radiation component  $N_{BG}(d, \alpha)$  which originates from diffuse scattered light in the experimental chamber.

The calculation of the SP radiation component  $N_{SP}(d, \alpha)$  requires some modifications of Eq. (2). First of all, the integration must be carried out over the angular acceptance  $\Delta\Phi = \pm 22 \text{ mrad}$  as defined by the longitudinal slit aperture above the grating. Second, the variation of the distance  $d$  of the electron beam above the grating as function of the  $x$  coordinate along the grating must be taken into account. Assuming that the distance  $d_k$  over the grating period  $k$  is constant the total intensity can be obtained by an incoherent

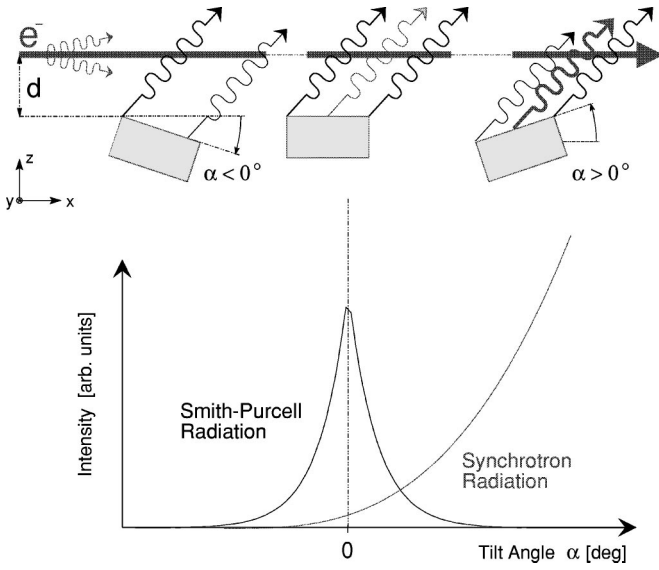


FIG. 5. Procedure to separate the diffracted synchrotron radiation contribution from Smith-Purcell radiation. As illustrated by the lower graph the intensity of both radiation components as function of the tilt angle  $\alpha$  of the grating exhibits distinct differences. Beam height has been adjusted.

summation over all  $(L/D-1)$  grating periods which yields

$$N_{SP}(d, \alpha) = A_{SP}(\alpha) \int_{\pi/2-1/2\Delta\Phi}^{\pi/2+1/2\Delta\Phi} d\Phi e^{-h_{int}^{-1} \sqrt{1+(\beta\gamma \cos \Phi)^2} d} \times \frac{1 - e^{-h_{int}^{-1} \sqrt{1+(\beta\gamma \cos \Phi)^2} L \sin \alpha}}{1 - e^{-h_{int}^{-1} \sqrt{1+(\beta\gamma \cos \Phi)^2} D \sin \alpha}}. \quad (4)$$

The integral must be calculated numerically. It is interesting to note that the intensity  $N_{SP}(d, \alpha)$  does not exhibit a pure

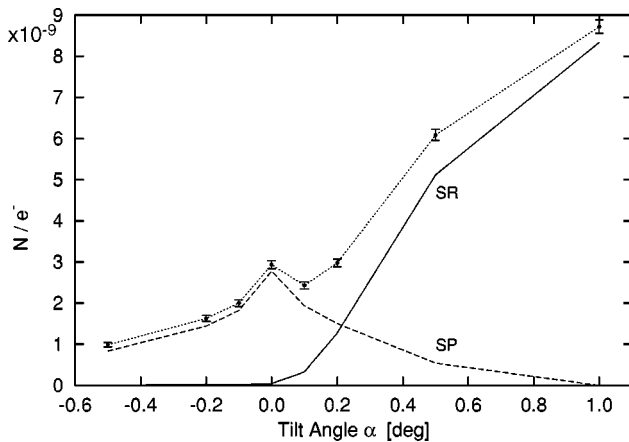


FIG. 6. Number of photons per electron as a function of the tilt angle  $\alpha$  of the grating. Shown are measurements for grating A at a wavelength  $\lambda = 546$  nm for a fixed distance  $d = 100$   $\mu\text{m}$  between electron beam and grating. The distribution resembles qualitatively the expectation, cf. Fig. 5. The individual Smith-Purcell and diffracted synchrotron radiation distributions, as separated by means of the fit procedure described in the text, are indicated.

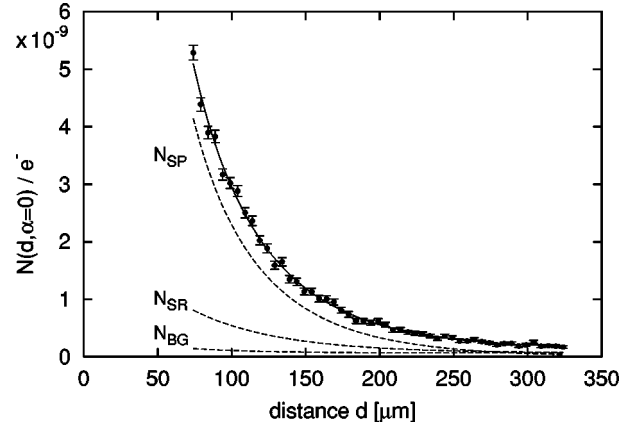


FIG. 7. Number of photons per electron  $N(d, \alpha=0)$  as a function of the beam distance  $d$  from the grating. The measurement was performed with grating A,  $\lambda = 546$  nm at a tilt angle  $\alpha = 0^\circ$ . The full line represents the best fit according to Eq. (9). The individual components for Smith-Purcell radiation  $N_{SP}(d, \alpha)$ , diffracted synchrotron radiation  $N_{SR}(d, \alpha)$ , and background radiation  $N_{BG}(d, \alpha)$  as given by Eqs. (4), (7), and (8), respectively, are also plotted.

exponential dependence as a function of the distance  $d$ . This is even not the case at a tilt angle  $\alpha = 0^\circ$  for which Eq. (4) reduces to

$$N_{SP}(d, \alpha=0) = A_{SP} \frac{L}{D} \int_{\pi/2-1/2\Delta\Phi}^{\pi/2+1/2\Delta\Phi} d\Phi e^{-h_{int}^{-1} \sqrt{1+(\beta\gamma \cos \Phi)^2} d}. \quad (5)$$

The integral can be solved analytically provided that the angular acceptance  $\Delta\Phi$  of the slit aperture is large in comparison to the angular width of the emitted SP radiation. This requirement is fulfilled in our experiment for  $d \geq 15$   $\mu\text{m}$ . The result is

$$N_{SP}(d, \alpha=0) = A_{SP} \frac{L}{D} \frac{2}{\beta\gamma} K_1(d/h_{int}), \quad (6)$$

with  $K_1(x)$  the modified Bessel function of first order. For arguments  $x = d/h_{int} \gg 1$  the modified Bessel function can be approximated by  $K_1(x) \rightarrow \sqrt{\pi/2x} e^{-x}$  [44], i.e. even for  $d \gg h_{int}$  the integrated intensity cannot be described by a pure exponential.

The SR component  $N_{SR}(d, \alpha)$  can best be studied at large tilt angles  $\alpha \approx 1^\circ$  for which the SP radiation component is small. We found that it can well be described by the function

$$N_{SR}(d, \alpha) = A_{SR}(\alpha) \exp(-d/\Lambda_{SR}) + B_{SR}(\alpha) \quad (7)$$

with  $\Lambda_{SR} \approx 60$   $\mu\text{m}$ .

The background component  $N_{BG}(d, \alpha)$  was obtained from separate measurements close to the maximum in the continuous part of the spectrum, cf. Fig. 3. It can be described for all tilt angles by the expression

$$N_{BG}(d, \alpha) = A_{BG}(\alpha) \exp(-d/\Lambda_{BG}) + B_{BG}(\alpha) \quad (8)$$

with typically  $\Lambda_{BG} \approx 45$   $\mu\text{m}$ .

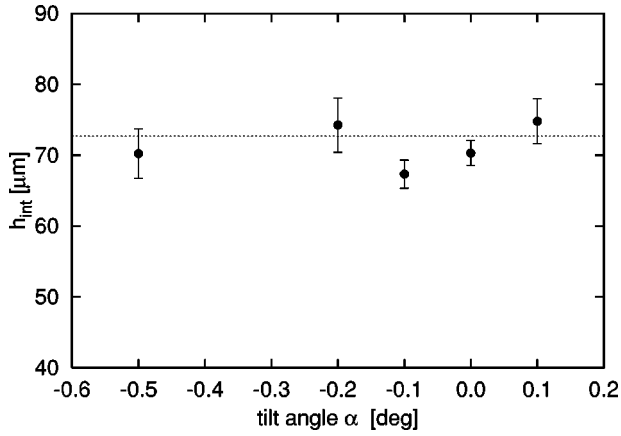


FIG. 8. Interaction length  $h_{int}$  as extracted for various tilt angles for grating A,  $\lambda = 546$  nm, and first diffraction order  $|n|=1$ . The value  $h_{int} = 72.7$   $\mu\text{m}$  as calculated by Eq. (3) is indicated by the dashed line.

The various radiation intensity spectra  $N(d, \alpha)$  were fitted with the function

$$N(d, \alpha) = N_{SP}(d, \alpha) + N_{SR}(d, \alpha) + N_{BG}(d, \alpha) \quad (9)$$

with  $N_{SP}(d, \alpha)$ ,  $N_{SR}(d, \alpha)$ , and  $N_{BG}(d, \alpha)$  as given by Eqs. (4), (7), and (8), respectively, and  $h_{int}$ ,  $A_{SP}(\alpha)$ ,  $A_{SR}(\alpha)$ , and  $B_{SR}(\alpha)$  as free parameters. A typical result of the best fit is shown in Fig. 7 for the example of tilt angle  $\alpha = 0^\circ$  together with the three radiation components  $N_{SP}$ ,  $N_{SR}$ , and  $N_{BG}$ .

Examples of the fit results for the interaction length  $h_{int}$  are shown in Figs. 8 and 9. The data exhibit no systematic deviation from a constant when the tilt angle of the grating is varied and agree well with the interaction length according to Eq. (3). This fact supplies additional confidence that the radiated intensity contains indeed a SP radiation contribution. Only for one measurement with grating B at  $\lambda = 546$  nm an

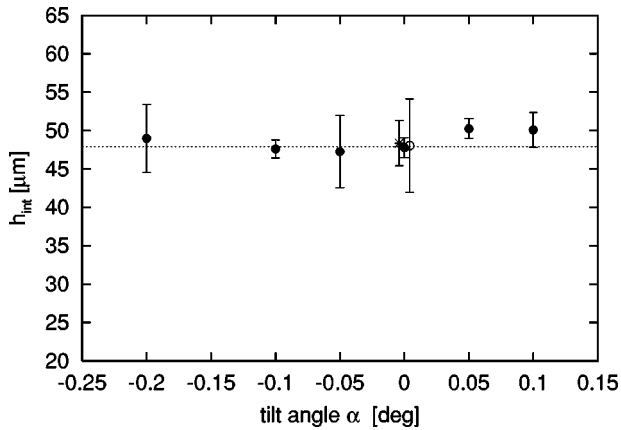


FIG. 9. Interaction length  $h_{int}$  as extracted for various tilt angles for grating B,  $\lambda = 360$  nm. Orders  $|n|=1$  ( $\times$ ),  $|n|=2$  ( $\circ$ ), and  $|n|=3$  ( $\bullet$ ). The data points for the first and second diffraction order at  $\alpha = 0^\circ$  have been shifted in the graph to  $\alpha = \pm 0.1^\circ$  for the sake of better representation. The value  $h_{int} = 47.9$   $\mu\text{m}$  as calculated by Eq. (3) is indicated by the dashed line.

additional radiation component of the type of Eq. (7) had to be added to obtain a good fit. The characteristic decay length  $\Lambda \approx 29$   $\mu\text{m}$  is consistent with the decay length of a known very weak beam halo component [45]. Therefore, it might be tempting to assume that this radiation component originates also from OTR production of beam halo electrons entering the grating grooves.

From these results together with the fact that the observed radiation also fulfills the dispersion relation Eq. (1) we conclude that in our experiment a SP radiation component has been identified unambiguously. In the next section its intensity will be extracted from the measurements and compared with theoretical predictions.

## IV. RESULTS AND DISCUSSION

### A. Radiation factors

The radiation factors  $|R_n|^2$  were determined at a tilt angle of the grating of  $\alpha = 0^\circ$  by a best fit to the data  $N(d, \alpha = 0)$  with Eq. (6) at fixed interaction lengths  $h_{int}$ , as given by Eq. (3), and

$$A_{SP} = |R_n|^2 \varepsilon_D N_e \alpha \frac{|n|L}{D} \frac{2}{\beta\gamma} \int_{\theta_n - \Delta\theta}^{\theta_n + \Delta\theta} d\theta \times F[\lambda(\theta) - \lambda_0] \frac{\sin^2 \theta}{(1/\beta - \cos \theta)^2}. \quad (10)$$

Here,  $\alpha$  is the fine structure constant,  $\varepsilon_D$  the detection efficiency with  $\varepsilon_D(546 \text{ nm}) = (2.0 \pm 0.6)\%$  (measured) and  $\varepsilon_D(360 \text{ nm}) = (8.3 \pm 2.5)\%$  (estimated),  $N_e$  the number of electrons with an uncertainty of 11.5%, and  $\theta_n$  the angle of observation at the central wavelength  $\lambda_0$ . The function  $F[\lambda(\theta) - \lambda_0]$ , with  $\lambda(\theta)$  as given by Eq. (1), describes the transmission characteristic of the color glass filters which was approximated by a normal distribution with FWHM  $\Delta\lambda = 30$  nm. The integration interval  $\Delta\theta = \pm 26$  mrad follows from the acceptance of the detection system.

The experimental radiation factors  $|R_n|^2$  are shown in Figs. 10 and 11. The error bars of the experimental  $|R_n|^2$  are dominated by the uncertainty of the detection efficiency  $\Delta\varepsilon_D = 30\%$ . For grating A at  $\lambda = 546$  nm and  $|n|=2$  no statistical significant SP radiation component was found. This result is represented in Fig. 11 as an upper limit, based on the 95% confidence level.

For the geometry in which the grating surface is aligned with respect to the beam axis our measurements can be compared with the theory of Van den Berg [34–39]. The calculated radiation factors based on the two-dimensional model described in Ref. [34] are shown in Figs. 10 and 11 as lines.

### B. Discussion

Comparing our experimental results with the calculations on the basis of Ref. [34] a fair overall agreement can be concluded. Deviations may not be surprising because the theory assumes a perfectly conducting grating surface. It is well known that on the basis of this assumption classical optical grating theories, which are the basis also of the Van

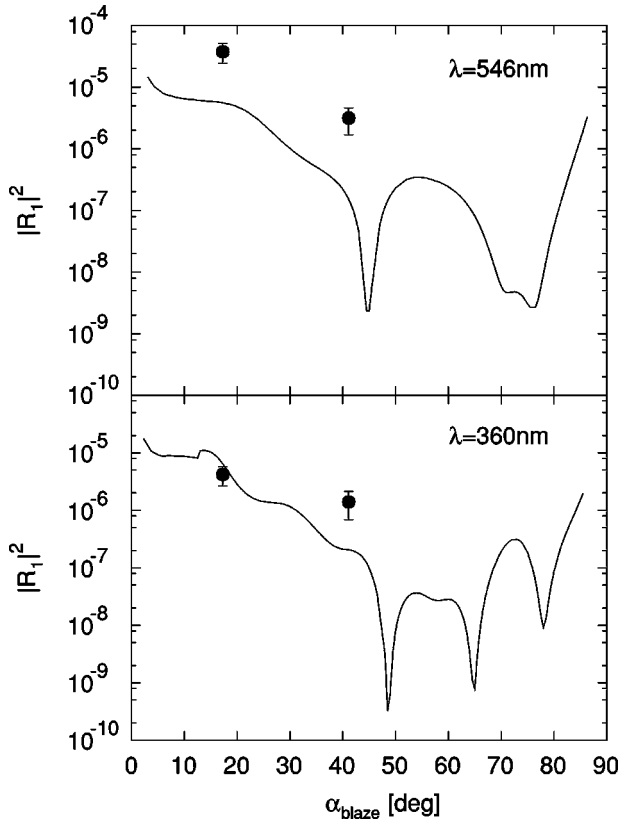


FIG. 10. Radiation factor  $|R_1|^2$  in first order as a function of the blaze angle for gratings A and B with grating period  $D=833$  nm. Experimental results of this paper are represented by (●) and calculations according to Ref. [34] by the solid line. The beam energy is 855 MeV.

den Berg theory, often fail to explain the reflectivity [46]. Therefore, it may well be that improved calculations, which take into account the finite conductivity of the grating surface, would even better agree with the experimental observations.

The striking feature of the results shown in Figs. 10 and 11 is that the radiation factors  $|R_n|^2$  are extremely small. We come back to this fact in Sec. V where optimal operational parameters of a SP radiation source are discussed.

It is also interesting to note that for the shallow grating C in Table I with  $\alpha_{blaze}=0.8^\circ$ ,  $D=9.09$   $\mu\text{m}$  the theory [34] predicted a radiation factor  $|R_1|^2=9.9\times 10^{-5}$ , see Fig. 12. However, no SP radiation component was found in the experimental data. The experimentally determined upper limit  $|R_1|^2<9.9\times 10^{-7}$  (95% confidence level) is clearly at variance with calculations based on the Van den Berg theory. The main problem connected with this theory is that, in general, extensive numerical calculations are required until finally the numerical solution of the integral equation converges. This is particularly difficult in the regime where the wavelength is small in comparison to the grating period [38]. In our calculations the convergence condition Eq. (40) in Ref. [34] was always fulfilled down to a level of 5%. In order to overcome the numerical difficulties and to explain eventually the discrepancy between experiment and theory a surface current model was developed which is described in the Appendix of

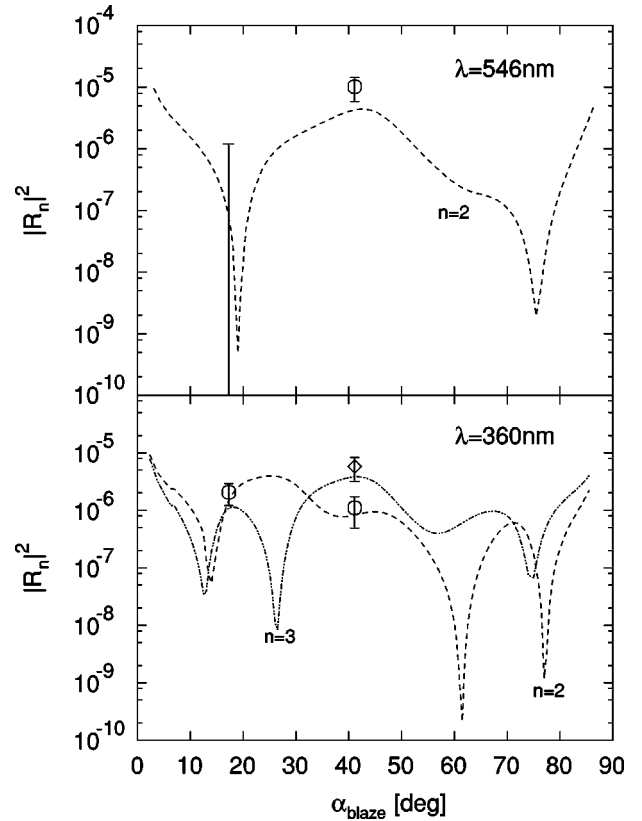


FIG. 11. Radiation factor  $|R_n|^2$  in second and third order as a function of the blaze angle. Experimental results are shown for gratings A and B with grating period  $D=833$  nm, (○) for  $|n|=2$  and (◇) for  $|n|=3$ . The experimental upper limit for  $|R_2(546\text{ nm})|^2$  for grating A is shown by the error bar. The dashed lines are calculations with Van den Berg's theory [34]. The beam energy is 855 MeV.

this paper. The approach used here is similar to that one published in Ref. [47]. Apart from an easier numerical han-

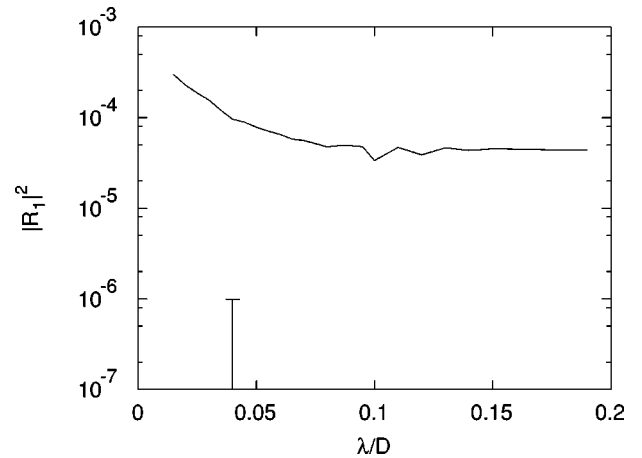


FIG. 12. Calculated radiation factor  $|R_1|^2$  for a shallow grating with blaze angle  $\alpha_{blaze}=0.8^\circ$  as a function of the normalized wavelength  $\lambda/D$ . The experimentally determined upper limit based on the 95% confidence level from a measurement with grating C at wavelength  $\lambda=360$  nm and  $|n|=1$  is indicated by the error bar.

ding, the advantage of this model in comparison to Van den Berg ones originates from the fact that it allows a clearer insight into the underlying physical processes. This model belongs to the category of scalar grating theories because no polarization effects which are responsible for the appearance of Wood's anomalies are included. It is well known from conventional optical grating theories that reasonable results are obtained for  $\lambda/D \leq 0.2$  [48] and presumably this holds also for SP radiation emission. With the ratio  $\lambda/D = 0.04$  for our experiment this condition is fulfilled. However, the intensity calculated with this model is still a factor of 50 higher than the upper limit derived from the experimental data, although it is lower in comparison to the Van den Berg theory. Since also the surface current model was deduced under the simplified assumption of an ideally conductive grating surface the still remaining large discrepancy may originate from this simplification which is discussed in more detail in the Appendix.

### V. ON OPTIMAL OPERATIONAL PARAMETERS OF SP RADIATION SOURCE

This section is devoted to a discussion of the optimum operational parameters of a SP radiation source. It is assumed that an electron beam with Lorentz factor  $\gamma$  and normalized emittance  $\varepsilon^N$  is available. The discussion will be carried out on the basis of Eq. (2) for  $\Phi = \pi/2$  and Eq. (3) assuming that the radiation factor  $|R_n|^2$  is a constant. In addition, the number of grating periods  $N_w$  is kept constant at a reasonably large value, e.g.,  $N_w = 100$ , rather than the grating length  $L$ . No further restrictions are imposed on the optimization procedure at this moment.

It can be seen from Eq. (2) that the emitted intensity depends very sensitively on the evanescent scaling length  $h_{int}$ , i.e., the coupling to the evanescent mode decreases exponentially if the electron passes over the grating in a distance much larger than  $h_{int}$ . In order to find the optimum coupling we start with the envelope equation for the vertical beam waist  $w_z(x)$  (see, e.g., [40])

$$\frac{w_z^2(x)}{w_{z0}^2} = 1 + \frac{(x - L/2)^2}{x_0^2} \quad (11)$$

with  $w_{z0}$  the beam spot size in the focus at  $x = L/2$ , cf. Fig. 1, and  $x_0$  given by

$$x_0 = w_{z0}^2 \frac{\beta\gamma}{\varepsilon^N/\pi}. \quad (12)$$

The distance  $d$  of the electron-beam axis above the grating is defined by the requirement that its waist just touches the grating at  $x = 0$  and  $L$ . Minimization of the distance  $d$  with respect to  $w_{z0}$  yields

$$d_{min} = \sqrt{L \frac{\varepsilon^N/\pi}{\beta\gamma}} = \sqrt{N_w D \frac{\varepsilon^N/\pi}{\beta\gamma}}. \quad (13)$$

A good coupling of the electron beam to the evanescent mode is achieved when the expectation value over the beam profile satisfies the inequality

$$\langle e^{-d_{min}/h_{int}} \rangle_{w_z(x)} = e^{-\kappa d_{min}/h_{int}} \geq e^{-1}. \quad (14)$$

In order to avoid the exact definition of the expectation value and elaborate calculations a coupling parameter  $\kappa \geq 1$  has been introduced. For the following estimates we use  $\kappa = 2$  which might be an adequate choice if the emittance of the electron beam is defined by its rms value. With Eqs. (13) and (14) a critical wavelength  $\lambda_{crit}$  can be defined in such a manner that the inequality (14) is satisfied for  $\lambda \geq \lambda_{crit}$ . With Eqs. (13) and (1) the critical wavelength can be rewritten as

$$\lambda_{crit} = \frac{(4\pi\kappa)^2}{(\beta\gamma)^3} \frac{N_w |n|}{1/\beta - \cos\theta} \varepsilon^N/\pi. \quad (15)$$

We still can dispose on the observation angle  $\theta$ . If it is chosen as

$$\cos\theta_{opt} = \beta = \sqrt{\gamma^2 - 1}/\gamma \quad (16)$$

the kinematical factor in Eq. (2),  $\sin^2\theta/(1/\beta - \cos\theta)^2$  in front of the exponential which now is a constant  $e^{-1}$ , is maximized. The final results are

$$\lambda \geq \lambda_{crit}^{opt} = \frac{(4\pi\kappa)^2}{\beta^2\gamma} N_w |n| \varepsilon^N/\pi \quad (17)$$

for the wavelength,

$$D_{opt} = |n| \lambda_{crit}^{opt} \beta \gamma^2 = (4\pi\kappa n)^2 N_w \frac{\gamma}{\beta} \varepsilon^N/\pi \quad (18)$$

for the grating period,

$$L_{opt} = N_w D_{opt} = (4\pi\kappa n N_w)^2 \frac{\gamma}{\beta} \varepsilon^N/\pi \quad (19)$$

for the grating length, and

$$\frac{dN}{d\Omega}|_{opt} = \alpha |n| N_w (\beta\gamma)^2 |R_n|^2 e^{-1} \quad (20)$$

for the SP photon number per electron and solid angle, all taken for the optimized critical wavelength  $\lambda_{crit}^{opt}$ . In Fig. 13(a) the critical wavelength  $\lambda_{crit}^{opt}$  is plotted as a function of the normalized emittance  $\varepsilon^N/\pi$  of the electron beam.

It is interesting to discuss these equations for the parameters  $\gamma = 1673$  and  $\varepsilon^N/\beta\gamma = 1 \pi$  nm rad of the Mainz Microtron MAMI. For  $N_w = 100$ ,  $|n| = 1$ ,  $\kappa = 2$  the results are  $\theta_{opt} = 0.6$  mrad,  $\lambda_{crit}^{opt} = 63 \mu\text{m}$ ,  $D_{opt} = 177$  m,  $L_{opt} = 17.68$  km, and  $dN_e/d\Omega|_{opt} = 7.5 \times 10^5 |R_n|^2/\text{sr}$  which are completely unreasonable. Extremely good normalized emittances would be required in order to achieve reasonable dimensions for such a SP radiation source. It is useless to say that such a device would not at all be competitive with a radiation source based on magnetic devices as, e.g., an undulator.

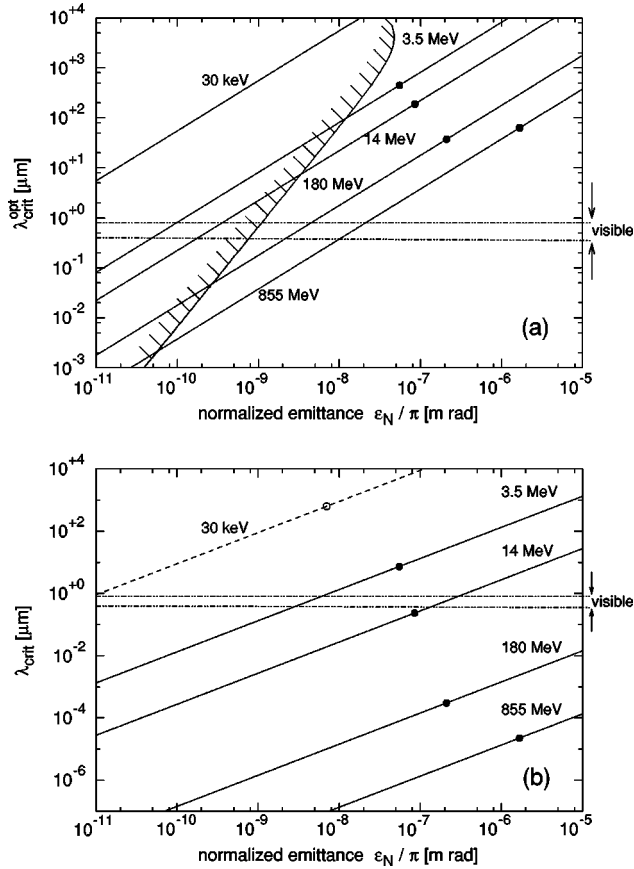


FIG. 13. Critical wavelength in first order  $|n|=1$  as a function of the normalized beam emittance for different beam energies (a) according to Eq. (17) at  $\theta_{opt}$  from Eq. (16), (b) according to Eq. (15) at an observation angle  $\theta=90^\circ$ . Solid lines are for  $N_w=100$ ,  $\kappa=2$ , the dashed line for  $N_w=73$ ,  $\kappa=1$ . Symbols (●) and (○) indicate the critical wavelengths  $\lambda_{crit}$  according to Eqs. (15) and (17) for beam emittances of the Mainz Microtron MAMI and the experiment of Urata *et al.* [50], respectively. The shadowed region is based on inequality (23).

The question arises under which circumstances a SP source might be superior to an undulator radiation source. In answering this question, we first note that the structure of Eq. (2) for the SP intensity has some striking similarities with its equivalent for undulator radiation (see also Ref. [49]). This can be seen by rewriting Eq. (2) in polar coordinates with  $\vartheta$  the polar and  $\varphi$  the azimuthal angle as measured with respect to the  $x$  and  $y$  axis, respectively. In the ultrarelativistic limit and at small angles  $\vartheta$  the result is

$$\frac{dN_{SP}}{d\Omega} = \alpha |n| N_w \gamma^2 \frac{4(\vartheta\gamma)^2}{[1+(\vartheta\gamma)^2]^2} \sin^2 \varphi |R_n|^2 \times \exp\left(-\frac{d}{h_{int}} \sqrt{1+(\vartheta\gamma)^2 \cos^2 \varphi}\right). \quad (21)$$

The equivalent equation for undulator radiation reads [40]

$$\frac{dN_{UR}}{d\Omega} = \alpha |n| N_w \gamma^2 \frac{4}{[1+K^2/2+(\vartheta\gamma)^2]^2} \times \left(\frac{K}{2}\right)^2 |n| F_J(n, K, \vartheta, \varphi). \quad (22)$$

The coupling factor  $(K/2)^2 |n| F_J(n, K, \vartheta, \varphi)$  for the undulator radiation with  $K$  the undulator parameter can well be in the order of one. The corresponding factor for SP radiation is  $\sin^2 \varphi |R_n|^2 \exp(-d/h_{int}) \sqrt{1+(\vartheta\gamma)^2 \cos^2 \varphi}$ .

A necessary condition for this factor to be also in the order of one is that an azimuthal angle  $\varphi = \pi/2$  is chosen, i.e., the radiation must be observed in the plane spanned by the  $x$  and  $z$  axis, and, in addition, that for the distance  $d$  between grating and electron beam  $d \leq h_{int}$  holds. The sufficient condition is that the radiation factor  $|R_n|^2$  is in the order of one. This requirement will be discussed below. The essential difference between the “kinematical” factors  $k_{SP} = 4(\vartheta\gamma)^2 [1+(\vartheta\gamma)^2]^{-2}$  and  $k_{UR} = 4[1+K^2/2+(\vartheta\gamma)^2]^{-2}$  for SP and undulator radiation, respectively, is that the SP radiation intensity always vanishes on axis. However, for an observation angle  $\vartheta \approx 1/\gamma$  the kinematical factor  $k_{SP}$  is in the same order of magnitude as  $k_{UR}$  at on-axis observation  $\vartheta = 0$ .

The remaining factors in Eqs. (21) and (22) are the same and it can be concluded that, provided the radiation factor  $|R_n|^2$  is also in the order of one, the SP radiation source is as powerful as the undulator radiation source. This holds if grating and undulator period lengths  $D$  and  $D_U$ , respectively, are the same. The corresponding wavelengths are  $|n|\lambda_{SP} = (D/2\gamma^2)[1+(\vartheta\gamma)^2]$  and  $|n|\lambda_{UR} = (D_U/2\gamma^2)[1+K^2/2+(\vartheta\gamma)^2]$  which actually agree for  $\vartheta\gamma=1$  for SP radiation and  $\vartheta\gamma=0$  for undulator radiation with a typical undulator parameter  $K = \sqrt{2}$ .

Accepting this, an essential advantage of a SP radiation source originates from the fact that short period gratings can be manufactured much easier than microundulators for which  $D_U \approx 8$  mm may be about the lower limit.

To proceed in the discussion we require somewhat arbitrarily that the grating period  $D$  should be shorter than about  $D_0 \approx 6$  mm. With this restriction we obtain from Eq. (18) that the beam emittance  $\varepsilon_0^N$  must fulfill the following inequality:

$$\frac{\varepsilon_0^N}{\pi} \leq \frac{D_0}{(4\pi\kappa n)^2} \frac{1}{N_w} \frac{\sqrt{\gamma^2-1}}{\gamma^2} =: C \frac{\sqrt{\gamma^2-1}}{\gamma^2}. \quad (23)$$

For  $\kappa=2$ ,  $N_w=100$ , and  $|n|=1$  the constant is  $C \approx 10^{-7}$  m. The inequality can only be fulfilled for  $\varepsilon_0^N/\pi \leq C/2 = 50$  nm rad for which  $\gamma$  is equal to  $\sqrt{2}$ . Thus, the worst emittance can be afforded for  $\gamma = \sqrt{2}$ , at all other beam energies better normalized emittances are required.

The emittance  $\varepsilon_0^N$ , corresponding to a period length  $D_0 \approx 6$  mm, is also shown in Fig. 13(a). An optimal radiation source must operate in the shadowed region. For short wavelengths, e.g.,  $\lambda = 25$  Å (water window), the electron beam with 855 MeV should have a normalized emittance  $\varepsilon^N/\pi$  as

low as  $6 \times 10^{-11}$  m rad which is completely out of the range for the Mainz Microtron MAMI and other currently existing accelerator facilities.

Beams with a normalized emittance  $\varepsilon^N/\pi \approx 10^{-8}$  m rad are available at electron microscope devices. As can be seen from Fig. 13(a) SP radiation with a wavelength  $\lambda \geq 60$   $\mu\text{m}$  can be produced at comparatively low-beam energies of  $E \leq 5$  MeV. Such a radiation source might be superior to an undulator radiation source. SP radiation production has been studied indeed with beams from an electron microscope [31,50]. The performance of such radiation sources may be further improved by employing magnetic guiding fields as it is common practice in millimeter wavelength devices (see, e.g., [10,11,13,14]).

The severe restriction on the operational parameters of a SP radiation source just discussed originates from the fact that both optimization conditions Eqs. (14) and (16) were demanded to be fulfilled simultaneously. In the discussion to follow, the restriction imposed on the observation angle is given up. At free disposal of the latter many operational conditions are conceivable at realistic grating periods. This is demonstrated in Fig. 13(b) for the observation angle  $\theta = \pi/2$ . Notice that the grating period is, according to Eq. (1),  $D = n\beta\lambda_{crit}$  which is in the order of the critical wavelength itself. However, a loss of intensity by about a factor of  $\gamma^2$  has to be paid for the choice of this observation angle which might be quite dramatic if the Lorentz factor  $\gamma$  is large. The reason is that the advantage of the relativistic forward boost has been given up.

Other optimization schemes have been discussed previously by Walsh [51] and Trotz *et al.* [52]. They came to the conclusion that higher-energy beams are capable of producing more narrowly focused and greater energy SP output than low-energy beams. In Ref. [52], the optimization procedure is based on the radiated energy at, in essence, a constant grating length while in our paper, the photon number at a constant number of grating periods has been optimized. In the former case, the optimum angle of observation in the ultrarelativistic case is  $\vartheta = \sqrt{2/\gamma}$  while we find according to Eq. (16)  $\theta_{opt} = 1/\gamma$ .

Clearly, the number of grating periods is the quantity of physical relevance since for a given observation angle it defines the emission spectrum

$$\frac{d^2N}{d\Omega d\omega/\omega} = 2\alpha n^2 N_w^2 \frac{\sin^2 \theta}{1/\beta - \cos \theta} \left( \frac{\sin \left( \pi N_w \frac{\omega - \omega_n}{\omega_n} \right)}{\pi N_w \frac{\omega - \omega_n}{\omega_n}} \right)^2 \times |R_n(\omega)|^2 e^{-d/h_{int}} \quad (24)$$

with  $\omega_n = 2\pi|n|c/[D(1/\beta - \cos \theta)]$ .

However, also the length of the grating may be subject to restrictions which could originate from experimental boundary conditions. Therefore, it may be appropriate to optimize according to the procedure proposed in Ref. [52]. Applying this procedure to Eq. (2), i.e., to the photon number rather than to the emitted energy, we obtain

$$\lambda^W = \frac{4\pi\kappa}{\beta\gamma} \sqrt{\frac{L\varepsilon^N/\pi}{\beta\gamma}} \quad (25)$$

for the wavelength,

$$D^W = 4\pi\kappa|n| \sqrt{\frac{L\varepsilon^N/\pi}{\beta\gamma}} \quad (26)$$

for the grating period,

$$N_w^W = \frac{1}{4\pi\kappa|n|} \sqrt{\frac{L\beta\gamma}{\varepsilon^N/\pi}} \quad (27)$$

for the number of grating periods and

$$\frac{dN^W}{d\Omega} = \frac{\alpha}{2\pi\kappa} \sqrt{\frac{L\beta\gamma}{\varepsilon^N/\pi}} (\gamma-1) |R_n|^2 e^{-1} \quad (28)$$

for the number of emitted photons per electron.

With a length of the grating of  $L_1 = 574$  mm which still might be reasonable for our experimental parameters  $\gamma = 1673$ ,  $\varepsilon^N/(\pi\beta\gamma) = 1$  nm rad,  $|n| = 1$ , and  $\kappa = 2$  we obtain  $\lambda_1^W = 360$  nm,  $D_1^W = 0.60$  mm,  $N_w^W = 953$ , and  $dN_1^W/d\Omega = 8.6 \times 10^3 |R_1|^2 \text{ sr}^{-1}$ . Comparing with the expected intensity according to Eq. (2) for grating A at  $\lambda = 360$  nm under our experimental conditions  $\theta = 55.4^\circ$ ,  $|n| = 1$ ,  $N_w = 30\,000$  the result is  $dN/d\Omega = 0.29 \times 10^3 |R_1|^2 \text{ sr}^{-1}$  which indeed is a factor of 30 smaller than the above-quoted number for the optimized grating.

For the shorter wavelength  $\lambda_2^W = 25$   $\text{\AA}$ , which might be of interest for practical applications (water window) the length of the grating scales down according to Eq. (25) to  $L_2 = L_1(\lambda_2^W/\lambda_1^W)^2 = 27.7$   $\mu\text{m}$ , and the grating period  $D^W$ , the grating number  $N_w^W$ , and the emitted photon number  $dN^W/d\Omega$  scale by the factor  $\sqrt{L_2/L_1} = \lambda_2^W/\lambda_1^W = 1/144$ . Let us compare the emitted photon number  $dN_2^W/d\Omega = 60 |R_1|^2 \text{ sr}^{-1}$  with the emission characteristics of an undulator with 10 poles, period length  $D_U = 9.33$  mm, and undulator parameter  $K = 1$  in first order  $|n| = 1$  at on-axis observation  $\vartheta = 0$ . The result is, according to Eq. (22),  $dN_{UR}/d\Omega \approx 3.6 \times 10^5 (K/2)^2 F_J(n, K, \vartheta, \varphi) \text{ sr}^{-1}$ . Assuming  $|R_1|^2 = (K/2)^2 F_J(n, K, \vartheta, \varphi) = 1$  this intensity is a factor of 6000 larger than the SP radiation. This result corroborates our previous conclusion that a SP radiation source does not perform better than an UR source in the wavelength range  $\lambda \leq 60$   $\mu\text{m}$ , even if a probably unrealistic radiation factor  $|R_1|^2 = 1$  is assumed. The reason is that also in the optimization scheme of Trotz *et al.* [52] the advantage of the relativistic forward boost has partly been given up leading to a reduction of the intensity of about a factor  $\gamma/2$ .

To produce radiation with wavelengths less than about 25  $\text{\AA}$  with an 855 MeV electron beam requires microundulators with periods  $D_U \leq 10$  mm which are difficult to construct. However, even in this case the SP radiation source is not advantageous since the number of periods will be, according to the optimization scheme of Ref. [52], less than

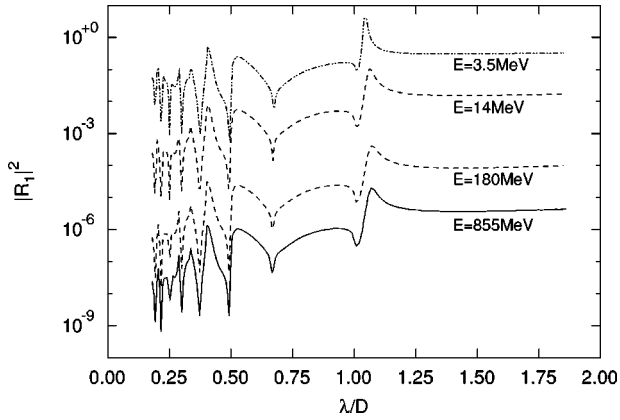


FIG. 14. Calculated functional dependence of the radiation factor  $|R_1|^2$  on the normalized wavelength  $\lambda/D$  according to Ref. [34] for a grating with  $\alpha_{blaze}=41.12^\circ$  (as for grating B). The quoted beam energies correspond to the different accelerator sections of the Mainz Microtron MAMI.

seven with the disadvantage that the spectral distribution at a fixed observation angle is very large.

As pointed out in Ref. [52] the large radiation factor  $|R_n|^2 \approx 1$  can be expected for strip gratings. A similar large value has been obtained for echelle-type gratings in this paper also for the surface current model, see the Appendix. However, it remains to be explored why the radiation factor is so large, independent on the Lorentz factor  $\gamma$  and the observation angle  $\vartheta$ , in comparison to calculations on the basis of the model of Van den Berg. As can be seen from Fig. 14 the radiation factors scale inversely proportional to  $\gamma^2$ , at least for  $\lambda/D \geq 0.2$ , and are in the order of  $10^{-6}$  at a beam energy of 855 MeV which is in fair agreement with our experimental findings.

## VI. CONCLUSION

The optical radiation emission has been investigated from diffraction gratings with echelle profiles using a low-emittance electron beam of an energy of 855 MeV. The spectrum is composed of various radiation components to which belongs (i) optical transition radiation emitted at close distance of the electron beam from the grating, (ii) Smith-Purcell radiation emitted at medium distances in the order of the interaction length  $h_{int}$  as given by Eq. (3), (iii) synchrotron radiation from upstream electron-beam optical elements which is diffracted by the grating, and (iv) background radiation from diffused scattered light in the experimental chamber.

These components could be isolated from each other by rather involved experimental procedures. The SP component has been identified by means of the dispersion relation Eq. (1) and the functional distance dependence of the intensity which is characterized by the interaction length Eq. (3). It was demonstrated that both dispersion relation and the evanescent scaling behavior of the intensity must be exploited to identify the SP radiation component unambiguously. It was shown that the  $\Phi$ -integrated intensity as a function of the beam height over the grating scales with a modified Bessel

function of the first kind rather than by a pure exponential. The intensity of the SP radiation component was compared with the Van den Berg theory and fair agreement was found for gratings with large or moderate blaze angles. However, the measured low intensity for a shallow grating with the angle  $\alpha_{blaze}=0.8^\circ$  and period length  $D=9.09 \mu\text{m}$  can neither be explained by the Van den Berg theory nor by the scalar model in the Appendix of this work or that one published in Ref. [47]. A general feature of SP radiation from optical diffraction gratings of echelle type at ultrarelativistic beam energies is the weakness of the radiation. The reason for that was found in the very small radiation factors  $|R_n|^2$ . These factors become large, according to Van den Berg's theory, only at low electron beam energies.

A detailed discussion of the emitted photon number per electron leads to the conclusion that a SP radiation source actually is not advantageous in comparison with an undulator radiation source for ultrarelativistic beam energies. However, a viable SP radiation source can probably be constructed in the spectral range  $\lambda \geq 60 \mu\text{m}$  employing electron beams with an energy of less than 5 MeV at a normalized emittance  $\varepsilon^N \approx 10 \pi \text{ nm rad}$ .

## ACKNOWLEDGMENTS

The authors would like to thank Dr. H. Barth, Dr. K. H. Brenzinger, Dr. S. Dambach, Dr. H. Kalinowsky, Dr. O. Ketting, Dr. Ch. Weinheimer, and Dr. R. Zahn for fruitful discussions and help during the course of the experiment. We gratefully acknowledge financial support from the Deutsche Forschungsgemeinschaft DFG (SFB 201 and Ba 1336/1–3).

## APPENDIX

This appendix describes a simple surface current model for the generation of Smith-Purcell (SP) radiation. The model correctly predicts the dispersion relation Eq. (1) and the interaction length of Eq. (3), i.e., the two properties that are at the focus of our experimental investigation, and it supports physical intuition in so far as its evaluation yields closed analytic expressions and as the resulting angular intensity distribution for emitted SP radiation can be written as a product of several factors with a clear physical interpretation. This is in contrast to the more rigorous theory of Van den Berg [37], which is formulated in terms of a boundary-value problem for partial differential equations and yields predictions only after extensive numerical calculations. A similar surface current model has been described by Brownell, Walsh, and Doucas [47], however, our derivation and our ansatz for the surface current differ slightly from theirs.

Our model is derived from the following consideration: An electron traveling parallel to a perfectly conducting plane is accompanied by an induced surface current density, but no radiation is emitted. Local deformations of the plane, such as the grooves of a reflection grating, represent obstacles that force the surface current into detours, thus acquiring components normal to the plane. Each obstacle in the path of the surface current therefore causes a current variation that is a

source of electromagnetic radiation, which in the far zone can be computed by well-known formulas.

Besides the surface current models described, there exist further scalar approaches for the description of SP radiation which are based on diffraction radiation [49,53–56]. While the surface current models are valid for arbitrary grating profiles, in the latter ones, only simplified structures are considered.

### 1. Ansatz for the surface current

According to Ref. [57] an electric charge  $q$  placed at rest at a distance  $d$  from the perfectly conducting plane  $z=0$  induces on this plane a charge density  $\sigma_0(x,y,z=0,t) = -(qd/2\pi)[x^2+y^2+d^2]^{-3/2}$ . By a Lorentz transformation we obtain the corresponding induced charge density for a charge  $q$  moving with velocity  $v$  in the direction of the positive  $x$  axis [ $\beta=v/c$ ,  $\gamma=(1-\beta^2)^{-1/2}$ ]

$$\sigma(x,y,z=0,t) = -\frac{1}{2\pi} \frac{\gamma q d}{[\gamma^2(x-vt)^2+y^2+d^2]^{3/2}} \quad (\text{A1})$$

and the associated induced surface current density is

$$J_x(x,y,z=0,t) = v\sigma(x,y,z=0,t), \quad J_y = J_z = 0. \quad (\text{A2})$$

No radiation is emitted. Translating this result into frequency space by means of a Fourier transformation with respect to time we obtain [cf. [44], p. 749, no. 6.699, Eq. (12)]

$$\begin{aligned} \sigma(x,y,z=0,\omega) &= \frac{1}{2\pi} \int_{-\infty}^{\infty} dt e^{+i\omega t} \sigma(x,y,z=0,t) \\ &= -\frac{q\omega d}{2\pi^2\gamma v^2} \frac{\exp\left(i\frac{\omega x}{v}\right)}{\sqrt{y^2+d^2}} K_1\left(\frac{\omega}{\gamma v} \sqrt{y^2+d^2}\right). \end{aligned} \quad (\text{A3})$$

Let us consider now the situation that the perfectly conducting plane  $z=0$  is deformed within a region  $\mathcal{G}$  into a reflection grating with grooves parallel to the  $y$  axis, so that the equation of the conducting surface is actually  $z=h(x)$  with  $h(x) \neq 0$ . The induced surface current has to be tangential to the deformed surface everywhere, i.e., it will acquire a component in the  $z$  direction and the components in the  $x$  and  $y$  directions may be changed. This requires

$$\frac{d}{dx} h(x) = h'(x) = \frac{J_z[x,y,z=h(x),\omega]}{J_x[x,y,z=h(x),\omega]}. \quad (\text{A4})$$

Considering specifically the échelette grating of Fig. 1 the  $j$ th period ( $j=1,2,\dots,N$ ) covers the coordinate range  $(j-1)D \leq x \leq jD$ . Within the  $j$ th period  $x=(j-1)D + \xi$  with  $0 \leq \xi \leq D$ . Given the blaze angle  $\alpha_b$  we have

$$h(x) = \begin{cases} \xi \tan \alpha_b & \text{for } 0 \leq \xi \leq D \cos^2 \alpha_b, \\ (D-\xi) \cot \alpha_b & \text{for } D \cos^2 \alpha_b \leq \xi \leq D, \end{cases}$$

and

$$h'(x) = \begin{cases} \tan \alpha_b & \text{for } 0 \leq \xi \leq D \cos^2 \alpha_b, \\ -\cot \alpha_b & \text{for } D \cos^2 \alpha_b \leq \xi \leq D. \end{cases}$$

Our model requires a plausible guess for the surface current. Equation (A3) suggests the ansatz (formally written as a three-dimensional current density)

$$\begin{aligned} j_x(x,y,z,\omega) &= -\delta[z-h(x)] \frac{q\omega}{2\pi^2\gamma v} e^{i\omega x/v} \frac{(d-z)}{\sqrt{y^2+(d-z)^2}} \\ &\quad \times K_1\left(\frac{\omega}{\gamma v} \sqrt{y^2+(d-z)^2}\right), \\ j_y(x,y,z,\omega) &= 0, \end{aligned} \quad (\text{A5})$$

$$j_z(x,y,z,\omega) = h'(x) j_x(x,y,z,\omega),$$

where  $\delta(z)$  denotes Dirac's  $\delta$  function.

### 2. Smith-Purcell radiation field

According to standard literature [57] the electromagnetic vector potential in Lorentz gauge generated by a three-dimensional current density distribution  $\mathbf{j}(\mathbf{x},\omega)$  is

$$\mathbf{A}(\mathbf{x},\omega) = \frac{1}{c} \int d^3x' \mathbf{j}(\mathbf{x}',\omega) \frac{e^{ikR}}{R} \quad (\text{A6})$$

with  $k=\omega/c$  and  $R=|\mathbf{x}-\mathbf{x}'|$ . At large distances  $r = \sqrt{x^2+y^2+z^2}$  and in the direction  $\mathbf{n}=(x/r,y/r,z/r)$  we have  $R \approx r - \mathbf{n} \cdot \mathbf{x}'$ , so that

$$\frac{e^{ikR}}{R} = \frac{e^{ikr}}{r} \cdot e^{-ik\mathbf{n} \cdot \mathbf{x}'}. \quad (\text{A7})$$

The unit vector  $\mathbf{n}$  can be expressed by the angles defined in Fig. 1 as

$$\mathbf{n} = (n_x, n_y, n_z) = (\sin \Phi \cos \theta, \cos \Phi, \sin \Phi \sin \theta). \quad (\text{A8})$$

Inserting our ansatz for the surface current Eq. (A5) and considering the échelette grating of Fig. 1 the integrations can be carried out explicitly. The integration with respect to  $z'$  is trivial. The integral with respect to  $y'$  can be obtained with the help of [cf. Ref. [44], p. 756, no. 6.726, Eq. (4)]

$$\begin{aligned} &\frac{2}{\pi} \text{Re} \left[ \int_0^{+\infty} dy' e^{-ik \cos \Phi y'} \frac{\tau K_1\left(\frac{k}{\beta\gamma} \sqrt{y'^2 + \tau^2}\right)}{\sqrt{y'^2 + \tau^2}} \right] \\ &= \frac{\beta\gamma}{k} \exp(-k\tau \sqrt{(\beta\gamma)^{-2} + \cos^2 \Phi}). \end{aligned} \quad (\text{A9})$$

The integration with respect to  $x'$  extending from 0 to  $L = ND$  reduces to the integral over a single groove multiplied by a coherence sum

$$C = \sum_{l=0}^{N-1} (e^{ikD(\beta^{-1} - \cos \theta \sin \Phi)})^l$$

$$= \frac{\exp[ikND(\beta^{-1} - \cos \theta \sin \Phi)] - 1}{\exp[ikD(\beta^{-1} - \cos \theta \sin \Phi)] - 1}. \quad (\text{A10})$$

As is well known from optics the coherence factor  $|C|^2$  is a rapidly oscillating function, that exhibits extremely narrow maxima at the positions where the condition

$$k_n D \left( \frac{1}{\beta} - \cos \theta \sin \Phi \right) = 2\pi n \quad (\text{A11})$$

is satisfied. The integer  $n$  is the order of the corresponding SP peak. The intermediate result valid for any shape of the grooves is

$$\mathbf{A}(\mathbf{x}, \omega) = -\frac{qD}{2\pi c} \exp\left[-\frac{kd}{\beta\gamma} \sqrt{1 + \beta^2 \gamma^2 \cos^2 \Phi}\right]$$

$$\times C \frac{e^{ikr}}{rD} \int_0^D dx' [\mathbf{e}_x + h'(x') \mathbf{e}_z]$$

$$\times \exp[kh(x')(\sqrt{(\beta\gamma)^{-2} + \cos^2 \Phi} - i \sin \theta \sin \Phi)$$

$$+ ikx'(\beta^{-1} - \cos \theta \sin \Phi)]. \quad (\text{A12})$$

The remaining integration depends on the shape of the grooves of the grating. In particular, for the échelette grating of Fig. 1 one finds

$$\mathbf{A}(\mathbf{x}, \omega) = -\frac{qD}{2\pi c} \exp\left[-\frac{kd}{\beta\gamma} \sqrt{1 + \beta^2 \gamma^2 \cos^2 \Phi}\right]$$

$$\times C(\mathbf{a}Q + \mathbf{a}'Q') \frac{e^{ikr}}{r}, \quad (\text{A13})$$

where  $\mathbf{a} = \cos \alpha_b \mathbf{e}_x + \sin \alpha_b \mathbf{e}_z$  and  $\mathbf{a}' = \sin \alpha_b \mathbf{e}_x - \cos \alpha_b \mathbf{e}_z$  are unit vectors tangential to the faces of the grooves, and the quantities  $Q$  and  $Q'$  are defined as

$$Q = \cos \alpha_b (e^\eta - 1) / \eta, \quad (\text{A14})$$

$$Q' = (\sin \alpha_b (e^{\eta'} - 1) / \eta') e^{ikD(\beta^{-1} - \cos \theta \sin \Phi)}, \quad (\text{A15})$$

with

$$\eta = kD \cos \alpha_b \sin \alpha_b \left( \sqrt{\frac{1}{\beta^2 \gamma^2} + \cos^2 \Phi} - i \sin \theta \sin \Phi \right)$$

$$+ ikD \cos^2 \alpha_b \left( \frac{1}{\beta} - \cos \theta \sin \Phi \right), \quad (\text{A16})$$

$$\eta' = kD \cos \alpha_b \sin \alpha_b \left( \sqrt{\frac{1}{\beta^2 \gamma^2} + \cos^2 \Phi} - i \sin \theta \sin \Phi \right)$$

$$- ikD \sin^2 \alpha_b \left( \frac{1}{\beta} - \cos \theta \sin \Phi \right). \quad (\text{A17})$$

At large distances  $r = \sqrt{x^2 + y^2 + z^2}$  and in the direction  $\mathbf{n} = (x/r, y/r, z/r)$  the electromagnetic fields associated with this vector potential are

$$\mathbf{E} = -ik \mathbf{n} \times (\mathbf{n} \times \mathbf{A}), \quad \mathbf{B} = \mathbf{n} \times \mathbf{E}. \quad (\text{A18})$$

### 3. Angular intensity distribution

The radiated energy flux as given by the Poynting vector becomes

$$\mathbf{S} = (c/4\pi) \mathbf{E} \times \mathbf{B} = (c/4\pi) (\mathbf{E} \cdot \mathbf{E}) \mathbf{n}$$

$$= (k^2 c/4\pi) |\mathbf{n}(\mathbf{n} \times \mathbf{A})|^2 \mathbf{n}. \quad (\text{A19})$$

The flux integrated over time is

$$\int_{-\infty}^{+\infty} dt \mathbf{S} = \frac{c}{4\pi} \mathbf{n} \int_{-\infty}^{+\infty} dt (\mathbf{E} \cdot \mathbf{E}) = c \mathbf{n} \int_0^\infty d\omega |\mathbf{E}(\mathbf{x}, \omega)|^2, \quad (\text{A20})$$

hence, the number of photons radiated per steradian and frequency interval is given by

$$\frac{dN_{\text{ph}}(\mathbf{n}, \omega)}{d\Omega d\omega} = \lim_{r \rightarrow \infty} \frac{c}{\hbar \omega} r^2 |\mathbf{E}|^2$$

$$= \lim_{r \rightarrow \infty} (c/\hbar \omega) (kr)^2 |\mathbf{n}(\mathbf{n} \times \mathbf{A})|^2. \quad (\text{A21})$$

Combining this with Eq. (A13) we obtain immediately the prediction

$$\frac{dN_{\text{ph}}(\mathbf{n}, \omega)}{d\Omega d\omega} = \frac{\alpha}{4\pi^2} \frac{(kD)^2}{\omega} |C|^2 |R|^2$$

$$\times \exp\left[-\frac{2kd}{\beta\gamma} \sqrt{1 + (\beta\gamma)^2 \cos^2 \Phi}\right], \quad (\text{A22})$$

where  $\alpha = q^2/(\hbar c)$  is the fine structure constant and

$$|R(\theta, \Phi, \omega)|^2 = |\mathbf{n} \times [\mathbf{n} \times (\mathbf{a}Q + \mathbf{a}'Q')]|^2 \quad (\text{A23})$$

is the structure factor that is obtained for the échelette grating. It is easily seen to vanish for blaze angles  $\alpha_b = 0$  and  $\alpha_b = \pi/2$ . At intermediate values of the blaze angle and with our experimental parameters it varies typically between 0 and 0.1.

Integrating over the frequency distribution around the  $n$ th order maximum  $\omega_n = k_n c$  all other terms are slowly varying and can be considered practically constant. We find

$$\int_{\omega_n - \Delta}^{\omega_n + \Delta} d\omega |C|^2 = \frac{2\pi c N}{D} \cdot \left( \frac{1}{\beta} - \cos \theta \sin \Phi \right)^{-1}. \quad (\text{A24})$$

Thus, the angular distribution of photons resulting from the  $n$ th-order SP peak is obtained as

$$\frac{dN_{\text{ph}}(\mathbf{n}, \omega_n)}{d\Omega} = \frac{\alpha n N}{\left(\frac{1}{\beta} - \cos \theta \sin \Phi\right)^2} |R(\theta, \Phi, \omega_n)|^2 \times \exp\left[-\frac{2kd}{\beta\gamma} \sqrt{1 + (\beta\gamma)^2 \cos^2 \Phi}\right]. \quad (\text{A25})$$

#### 4. Discussion

Unfortunately, the structure factor (A23) following from the surface current ansatz (A5) turns out to be much larger than found by our experiments (typically  $10^{-6}$ ). Let us discuss possible reasons for this. Our ansatz (A5) has been deduced from a static equilibrium situation as seen by a moving observer. Aside from the assumption of perfect conductivity this picture presupposes that the time necessary to build up the induced current is extremely short on the time scale in which the field of the beam electron changes in the laboratory frame. This assumption seems plausible for electron beams moving at nonrelativistic speeds, but it becomes questionable for an ultrarelativistic beam. We rather expect that the ultrarelativistic electron traveling parallel to the metal surface is accompanied by a small spot of polarization

(i.e., an electric dipole density), because conduction electrons of the metal are pushed away from the surface into the interior of the metal. The depletion of electrons on the metal surface, traveling with the beam electron, mimics a surface current of positive charge carriers accompanying the beam electron, while at the same time a compensating current of negative charge carriers (electrons) travels further inside the metal, in other words, we deal effectively with a current of induced electric dipole density. Assuming the two currents of opposite electric charge to be at a distance  $\Delta$  and using ansatz (A5) for each of these the angular distribution of SP photons picks up another factor

$$\left(1 - \exp\left[-\frac{k\Delta}{\beta\gamma} \sqrt{1 + (\beta\gamma)^2 \cos^2 \Phi}\right]\right)^2 \approx \left(\frac{k\Delta}{\beta\gamma} \sqrt{1 + (\beta\gamma)^2 \cos^2 \Phi}\right)^2. \quad (\text{A26})$$

With parameters typical for our experiment,  $\Phi = \pi/2$ ,  $\lambda = 546$  nm,  $\beta \approx 1$ , and  $\gamma = 1672$  a choice of  $\Delta = 100$  nm would result in a factor of  $\approx 10^{-6}$  and would therefore reduce the structure factor (A23) to a size compatible with the experiment.

- 
- [1] I. M. Frank, *Izv. Akad. Nauk SSSR, Ser. Fiz.* **6**, 3 (1942).  
[2] S. J. Smith and E. M. Purcell, *Phys. Rev.* **92**, 1069 (1953).  
[3] W. W. Salisbury, *J. Opt. Soc. Am.* **60**, 1279 (1970).  
[4] J. P. Bachheimer, *Phys. Rev. B* **6**, 2985 (1972).  
[5] E. L. Burdette and G. Hughes, *Phys. Rev. A* **14**, 1766 (1976).  
[6] A. Gover, P. Dvorkis, and U. Elisha, *J. Opt. Soc. Am. B* **1**, 723 (1984).  
[7] I. Shih, W. W. Salisbury, D. L. Masters, and D. B. Chang, *J. Opt. Soc. Am. B* **7**, 345 (1990).  
[8] I. Shih *et al.*, *J. Opt. Soc. Am. B* **7**, 351 (1990).  
[9] I. Shih *et al.*, *Opt. Lett.* **15**, 559 (1990).  
[10] F. Rusin and G. Bogomolov, *Proc. IEEE* **57**, 720 (1969).  
[11] K. Mizuno, S. Ono, and Y. Shibata, *IEEE Trans. Electron Devices* **20**, 749 (1973).  
[12] J. M. Wachtel, *J. Appl. Phys.* **50**, 49 (1979).  
[13] D. E. Wortman, R. P. Leavitt, H. Dropkin, and C. A. Morrison, *Phys. Rev. A* **24**, 1150 (1981).  
[14] E. M. Marshall, P. M. Phillips, and J. E. Walsh, *IEEE Trans. Plasma Sci.* **16**, 199 (1988).  
[15] L. Schächter and A. Ron, *Phys. Rev. A* **40**, 876 (1989).  
[16] B. Hafizi, P. Sprangle, and A. Fisher, *Nucl. Instrum. Methods Phys. Res. A* **341**, 269 (1994).  
[17] A. Hirata and T. Shiozawa, *Electron. Commun. Jpn., Part 2: Electron.* **80**, 30 (1997).  
[18] K. Mizuno, S. Ono, and O. Shimoe, *Nature (London)* **253**, 184 (1975).  
[19] M. C. Lampel, *Nucl. Instrum. Methods Phys. Res. A* **385**, 19 (1997).  
[20] D. Nguyen, *Nucl. Instrum. Methods Phys. Res. A* **393**, 514 (1997).  
[21] T. di Francia, *Nuovo Cimento* **16**, 61 (1960).  
[22] K. Ishiguro and T. Takao, *Opt. Acta* **8**, 25 (1961).  
[23] I. Palócz and A. A. Oliner, *Proc. IEEE* **55**, 46 (1967).  
[24] J. C. McDaniel, D. B. Chang, J. E. Drummond, and W. W. Salisbury, *Appl. Opt.* **28**, 4924 (1989).  
[25] G. Doucas *et al.*, *Phys. Rev. Lett.* **69**, 1761 (1992).  
[26] K. J. Woods *et al.*, *Phys. Rev. Lett.* **74**, 3808 (1995).  
[27] K. Ishi *et al.*, *Phys. Rev. E* **51**, R5212 (1995).  
[28] J. H. Brownell *et al.*, *Nucl. Instrum. Methods Phys. Res. A* **393**, 323 (1997).  
[29] Y. Shibata *et al.*, *Phys. Rev. E* **57**, 1061 (1998).  
[30] J. H. Brownell *et al.*, *J. Phys. D* **30**, 2478 (1997).  
[31] M. Goldstein *et al.*, *Appl. Phys. Lett.* **71**, 452 (1997).  
[32] G. Kube, Dissertation, Institut für Kernphysik, Universität Mainz, 1998 (in German).  
[33] J. Ahrens *et al.*, *Nucl. Phys.* **4**, 5 (1994).  
[34] P. M. Van den Berg, *J. Opt. Soc. Am.* **63**, 689 (1973).  
[35] P. M. Van den Berg, *J. Opt. Soc. Am.* **63**, 1588 (1973).  
[36] P. M. Van den Berg, *J. Opt. Soc. Am.* **64**, 325 (1974).  
[37] P. M. Van den Berg, *Appl. Sci. Res.* **24**, 261 (1971).  
[38] O. Haeberlé, P. Rullhusen, J. M. Salomé, and N. Maene, *Phys. Rev. E* **49**, 3340 (1994).  
[39] O. Haeberlé, P. Rullhusen, J. M. Salomé, and N. Maene, *Phys. Rev. E* **55**, 4675 (1997).  
[40] C. A. Brau, *Free-Electron Lasers* (Academic Press, Boston, 1990).  
[41] H. Schöpe, Dissertation, Institut für Kernphysik, Universität Mainz, 1999 (in German).  
[42] P. Henri *et al.*, *Phys. Rev. E* **60**, 6214 (1999).  
[43] Y. Takakura and O. Haeberlé, *Phys. Rev. E* **61**, 4441 (2000).  
[44] I. S. Gradshteyn and I. M. Ryzhik, *Table of Integrals, Series, and Products*, 4th ed. (Academic Press, New York, 1965).  
[45] H. Euteneuer *et al.*, in *Proceedings of the 5th European Particle Accelerator Conference (EPAC94)*, edited by V. Suller

- and C. Petit-Jean-Genaz, (Wold Scientific, London, 1994), Vol. 1, p. 506.
- [46] *Electromagnetic Theory of Gratings*, edited by R. Petit (Springer-Verlag, Berlin, 1980).
- [47] J. H. Brownell, J. Walsh, and G. Doucas, Phys. Rev. E **57**, 1075 (1998).
- [48] E. G. Loewen, M. Nevière, and D. Maystre, Appl. Opt. **16**, 2711 (1977).
- [49] G. N. Naumenko, A. P. Potylitsyn, and O. V. Chefonov, Nucl. Instrum. Methods Phys. Res. B **173**, 88 (2001).
- [50] J. Urata *et al.*, Phys. Rev. Lett. **80**, 516 (1998).
- [51] J. E. Walsh, Nucl. Instrum. Methods Phys. Res. A **445**, 214 (2000).
- [52] S. R. Trotz, J. H. Brownell, J. E. Walsh, and G. Doucas, Phys. Rev. E **61**, 7057 (2000).
- [53] M. J. Moran, Phys. Rev. Lett. **69**, 2523 (1992).
- [54] A. P. Potylitsyn, Phys. Lett. A **53**, 112 (1998).
- [55] A. P. Potylitsyn, Nucl. Instrum. Methods Phys. Res. B **145**, 60 (1998).
- [56] A. P. Potylitsyn, P. V. Karataev, and G. A. Naumenko, Phys. Rev. E **61**, 7039 (2000).
- [57] J. D. Jackson, *Classical Electrodynamics*, 2nd ed., (Wiley, New York, 1975).